

Critical appraisal of excited state nonadiabatic dynamics simulations of 9H-adenine)

Mario Barbatti, Zhenggang Lan, Rachel Crespo-Otero, Jaroslaw J. Szymczak, Hans Lischka, and Walter Thiel

Citation: *The Journal of Chemical Physics* **137**, 22A503 (2012); doi: 10.1063/1.4731649View online: <http://dx.doi.org/10.1063/1.4731649>View Table of Contents: <http://scitation.aip.org/content/aip/journal/jcp/137/22?ver=pdfcov>Published by the [AIP Publishing](#)

Articles you may be interested in[Electronic structure and UV spectrum of hexachloroplatinate dianions in vacuo a\)](#)J. Chem. Phys. **139**, 194310 (2013); 10.1063/1.4830407[The electronic structure of the triiodide ion from relativistic correlated calculations: A comparison of different methodologies](#)J. Chem. Phys. **133**, 064305 (2010); 10.1063/1.3474571[An investigation of the molecular geometry and electronic structure of nitril chloride by a combination of rotational spectroscopy and ab initio calculationsa\)](#)J. Chem. Phys. **128**, 204305 (2008); 10.1063/1.2920487[A vacuum ultraviolet pulsed field ionization-photoelectron study of cyanogen cation in the energy range of 13.2–15.9 eV\)](#)J. Chem. Phys. **123**, 144302 (2005); 10.1063/1.2037607[A new pathway for the rapid decay of electronically excited adenine](#)J. Chem. Phys. **122**, 104314 (2005); 10.1063/1.1861452

**AIP** | Journal of
Applied Physics

Journal of Applied Physics is pleased to
announce **André Anders** as its new Editor-in-Chief

Critical appraisal of excited state nonadiabatic dynamics simulations of 9H-adenine^{a)}

Mario Barbatti,^{1,b)} Zhenggang Lan,^{2,b)} Rachel Crespo-Otero,¹ Jaroslaw J. Szymczak,^{3,4} Hans Lischka,^{4,5} and Walter Thiel^{1,b)}

¹Max-Planck-Institut für Kohlenforschung, Kaiser-Wilhelm-Platz 1, 45470 Mülheim, Germany

²Qingdao Institute of Bioenergy and Bioprocess Technology, Chinese Academy of Sciences, Qingdao 266101, People's Republic of China

³Department of Chemistry, University of Basel, Klingelbergstrasse 80, 4056 Basel, Switzerland

⁴Institute for Theoretical Chemistry, University of Vienna, Währinger Str. 17, 1090 Vienna, Austria

⁵Department of Chemistry and Biochemistry, Texas Tech University, Lubbock, Texas 79409-1061, USA

(Received 25 April 2012; accepted 8 June 2012; published online 13 July 2012)

In spite of the importance of nonadiabatic dynamics simulations for the understanding of ultrafast photo-induced phenomena, simulations based on different methodologies have often led to contradictory results. In this work, we proceed through a comprehensive investigation of on-the-fly surface-hopping simulations of 9H-adenine in the gas phase using different electronic structure theories (*ab initio*, semi-empirical, and density functional methods). Simulations that employ *ab initio* and semi-empirical multireference configuration interaction methods predict the experimentally observed ultrafast deactivation of 9H-adenine with similar time scales, however, through different internal conversion channels. Simulations based on time-dependent density functional theory with six different hybrid and range-corrected functionals fail to predict the ultrafast deactivation. The origin of these differences is analyzed by systematic calculations of the relevant reaction pathways, which show that these discrepancies can always be traced back to topographical features of the underlying potential energy surfaces. © 2012 American Institute of Physics. [<http://dx.doi.org/10.1063/1.4731649>]

I. INTRODUCTION

The availability of computational methods for nonadiabatic dynamics simulations in the gas and condensed phase has played a major role in our understanding of photo-induced molecular processes.^{1–4} Concepts like competition between reaction pathways or nonadiabatic events near the crossing seam are now part of the repertoire of ideas commonly employed to understand ultrafast processes.⁵ In spite of the importance of dynamics simulations to shape this qualitative knowledge, a less recognized fact is that much of the quantitative information that has been published in this field so far is under dispute.^{4,6–8} Dynamics simulations based on different methodologies have often led to different or even contradictory results. Factors that may be responsible for this situation include not only the dynamics methodologies themselves but also different ways of comparing to experimental data, and, most critically, topographical differences in the potential energy surfaces obtained by different electronic structure methods. In this paper, we will focus on the nonadiabatic dynamics simulations of gas-phase 9H-adenine (hereafter: adenine), one important example where different electronic structure methods have produced contradictory results.^{9–12}

As typical for small aromatic systems, adenine and the other nucleobases are good chromophores in the UV range.¹³

They show, however, low fluorescence quantum yields and very short excited state lifetimes, which are in the order of few picoseconds or less.^{14–16} This is an unequivocal indication that the deactivation of UV-excited nucleobases takes place via internal conversion at conical intersections. Many theoretical studies have been dedicated to mapping the possible reaction pathways for internal conversion of nucleobases.^{17–23} More recently, a significant number of investigations have employed nonadiabatic dynamics simulations to clarify the role of the various available reactions pathways under several environmental conditions. Most of them have applied the trajectory surface-hopping method based on *ab initio*,^{11,12,24–28} density functional theory (DFT),^{10,29–32} and semi-empirical^{9,33–40} surfaces, while some of them have employed mean field,⁴¹ multiple spawning,^{42,43} and wave packet propagation^{44–47} methods.

Adenine has the most extensive collection of time-dependent experimental results among the nucleobases covering a range of pump wavelengths from 277 to 200 nm.^{13,15,16,48–56} In the case of gas-phase adenine, the excited state decay shows two time constants around 0.1 ps and 1 ps.^{15,16,51–53} The latter is dependent on the pump wavelength, ranging from 0.7 ps at 200.5 nm to 1.0 ps at 265.1 nm.⁵⁵ Measurements at 277 nm showed much longer lifetimes, around 9 ps,⁴⁸ indicating that, at very low excitation energies, relatively large barriers might need to be overcome before internal conversion takes place. At 267 nm, neither single methylation^{16,50,52,53} nor deuteration⁵⁰ has significant impact on the lifetime, implying a minor role of the hydrogen detachment for the internal conversion. Total kinetic energy

^{a)}Contributed paper. Published as part of the Special Topic Issue on Nonadiabatic Dynamics.

^{b)}Authors to whom correspondence should be addressed. Electronic addresses: barbatti@kofo.mpg.de, lanzg@qibebt.ac.cn, and thiel@kofo.mpg.de.

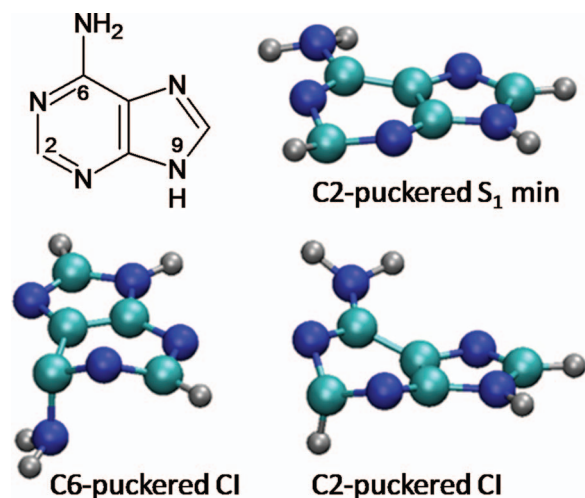


FIG. 1. Geometries of the C2-puckered S_1 minimum and of the main S_1/S_0 conical intersections in 9H-adenine.

release investigations showed that hydrogen detachment will become relevant for pump wavelengths below 200 nm.^{55,57} On the other hand, the lifetime of 2-aminopurine is 30 ps at 267 nm, which suggests that C6 and C2 distortions of the pyrimidine ring are related to the internal conversion.^{16,21}

The computational search for stationary points, reaction pathways, and conical intersections on the excited state surfaces of adenine has revealed a set of three main channels that could be responsible for the ultrafast deactivation.^{17,19,20,23} The first pathway, corresponding to a puckering of the C2 atom in relation to the ring plane, brings adenine to a C2-puckered S_1/S_0 conical intersection, whose geometry is depicted in Fig. 1. On the second pathway, atoms C6 and N1 are distorted out of the ring plane, giving rise to the C6-puckered

conical intersection (also shown in Fig. 1). Characteristically, at the geometry of this conical intersection, the amino group is also strongly distorted out of the ring plane. The third pathway occurs along the hydrogen detachment from N9, which also promotes a S_1/S_0 crossing.

Several theoretical studies have addressed the deactivation of adenine by dynamics simulations in the gas phase,^{9–12,37,41} within water,^{10,38} and in nucleic acid environments.^{37,39,40} The main results of these investigations are surveyed in Table I. We can see that even though most of the simulations in the gas phase have been able to predict the ultrafast deactivation of adenine,^{9,11,12,37,41} they are far from a consensus concerning the predominant mechanism. It is also remarkable that the time-dependent density functional tight-binding method (TDDFTB) completely fails to predict the ultrafast deactivation in the gas phase within a reasonable time.¹⁰

These discrepancies have been largely ignored in previous works, probably because of a missing common ground for comparing the results obtained with different methods by different research groups. In this paper, we address these issues by carrying out static calculations and dynamics simulations, in which we employ several different electronic structure methods while using the same methodological tools for the analysis of the results. Our comparisons cover static (excitation energies, reaction paths) and dynamic (lifetimes, mechanisms) properties obtained from some of the most popular methods currently available for excited state calculations.

The present study includes a detailed investigation of adenine dynamics in the gas phase with the *ab initio* multireference configuration interactions with single excitations (MRCIS), the multireference configuration interaction based on the semi-empirical orthogonalization model 2 Hamiltonian (OM2/MRCI), and the time-dependent density functional

TABLE I. Summary of results from dynamics simulations of UV-excited adenine with different methods.

Dynamics	Electronic structure	Phase	Main pathway	τ (ps)	References
Surf. hopp.	MRCIS-1n	Gas	C2-puck (100%)	0.44–0.77 ^a	11, 12
Surf. hopp.	MRCIS-2n	Gas	C2-puck (79%)	0.53	This work
Surf. hopp.	OM2/MRCI (4 refs) ^b	Gas	C6-puck (90%)	0.56	9
Surf. hopp.	OM2/MRCI (5 refs) ^b	Gas	C6-puck (93%)	0.64	This work
Surf. hopp.	OM2/MRCI (5 refs) ^c	Gas	C6-puck (95%)	0.90	This work
Surf. hopp.	OM2/MRCI	Water	C6-puck (>90%)	0.41	38
Surf. hopp.	OM2/MRCI	DNA-1 strd.	C6-puck (57%)	5.7	39
Surf. hopp.	OM2/MRCI	DNA-2 strd.	C2-puck (64%)	4.1	39
Surf. hopp.	Several functionals	Gas	Planar	$\gg 1$	This work
Surf. hopp.	TDDFTB	Water	not given	0.2	10
Surf. hopp.	TDDFTB	Gas	not given	11	10
Surf. hopp.	FOMO/AM1	Gas ^d	C6-puck	$\sim 1.6^e$	37
Surf. hopp.	FOMO/AM1	AT pair ^d	C6-puck	$\sim 1.6^e$	37
Mean field	DFTB	Gas	C6-puck	1.05 ^f	41
			C2-puck	1.36 ^g	

^aDepending on the initial energy.

^bWithout decoherence correction.

^cWith decoherence correction.

^dAdenine nucleoside with initial geometry as in DNA.

^eExtrapolation from the reported data with a single exponential fitting function.

^fInitial energy: 5.0 eV.

^gInitial energy: 4.8 eV.

theory (TDDFT) employing six different functionals. Simulations with the *ab initio* MRCIS and with the semi-empirical OM2/MRCI levels predict the experimentally observed ultrafast deactivation of adenine with similar time scales, however, through different internal conversion channels. All simulations with TDDFT fail to predict the ultrafast deactivation.

II. COMPUTATIONAL DETAILS

Details on computational methods, procedures, and approximate computation times are given in the supplemental material.⁵⁸ In this section, we only provide a brief summary.

TDDFT: Electronic structure calculations were performed with the PBE,⁵⁹ B3LYP,^{60,61} PBE0,⁶² BHLYP,⁶³ CAM-B3LYP,⁶⁴ and M06-HF⁶⁵ functionals. Vertical excitations and reaction paths were computed with the aug-cc-pVDZ basis set.⁶⁶ Dynamics was performed with the split-valence plus polarization (SVP) basis set⁶⁷ augmented by a set of diffuse *sp* functions added to C and N atoms (SVP-aug).

OM2/MRCI: The excited states were described by a MRCI treatment⁶⁸ based on the semi-empirical OM2 Hamiltonian.^{69–72} The active space consisted of 12 electrons in 10 orbitals ($3n$, 3π , $3\pi^*$, $1\sigma^*$). The inclusion of $1\sigma^*$ was found to improve the numerical robustness of the nonadiabatic dynamics simulations without affecting the results significantly. In the MRCI treatment, five reference configurations were considered.

CC2: The resolution-of-identity coupled-cluster to second-order method (RI-CC2) (Refs. 73–75) was applied with the aug-cc-pVDZ basis set.

CASPT2: Ground- and excited state energies were computed with the complete active space second-order perturbation theory in its single-state (SS) and multi-state (MS) versions.⁷⁶ The complete active space self-consistent field (CASSCF) calculations employed an active space composed of 16 electrons in 12 orbitals [CASSCF(16,12), ($3n$, 5π , $4\pi^*$)]. A total of 5 electronic states were included in the state-averaging procedure. Calculations were performed including the IPEA shift⁷⁷ (0.25 a.u.) and an imaginary level shift (0.2 a.u.). The aug-cc-pVDZ basis set was adopted in these calculations.

DFT/MRCI:⁷⁸ MRCI calculations based on Kohn-Sham orbitals were performed with the BHLYP functional. The aug-cc-pVDZ basis set was adopted in these calculations. Auxiliary basis functions for the RI approximation of two-electron integrals were taken from the Turbomole library.^{79,80}

MRCIS: *Ab initio* MRCI calculations were performed with a CAS space including 10 electrons in 8 orbitals ($2n$, 3π , $3\pi^*$) and with state averaging over 5 states. The reference space for the CI procedure was composed of 6 electrons in 4 orbitals. The CI space was built by allowing all single excitations from the reference CSF's (excluding $1s$ -core orbitals). The 6-31G* basis set⁸¹ was employed. This level will be called MRCIS-2n, in distinction to the MRCIS-1n level employed in

Ref. 24, which included only one *n* orbital in the CAS space.

Surface-hopping dynamics simulations were performed with *ab initio* MRCIS, OM2/MRCI, and TDDFT. The velocity-Verlet algorithm was employed to propagate nuclear trajectories up to 1.0 ps (1.5 ps in the case of MRCIS-2n) with a time step of 0.5 fs (MRCIS and TDDFT) or 0.1 fs (OM2/MRCI). Quantum equations were integrated with a time step of 0.01 fs (MRCIS and TDDFT) or 0.001 fs (OM2/MRCI) using interpolation between the time steps of the classical dynamics. With MRCIS and TDDFT, time-dependent coefficients were corrected for decoherence effects ($\alpha = 0.1$ hartree).⁸² OM2/MRCI dynamics was performed without and with decoherence correction ($\alpha = 0.1$ hartree). In all simulations, the hopping probabilities at each time step were computed by Tully's fewest switches algorithm.⁸³

TDDFT dynamics simulations were performed with numerical computation of nonadiabatic coupling terms⁸⁴ as described in Ref. 85. A total of 176 trajectories were computed. The TDDFT jobs terminated with Kohn-Sham convergence failures when the S_1 state approached the ground state to within an energy gap smaller than about 0.2 eV. This breaking time was taken as an estimate (i.e., a lower bound) for the $S_1 \rightarrow S_0$ transition time (assuming an immediately following internal conversion). Because of these DFT limitations, we could properly simulate only hopping events between excited states.

In the case of OM2/MRCI, nonadiabatic couplings were calculated analytically,^{68,69,86} and 90 trajectories were computed. For MRCIS-2n, nonadiabatic couplings were also calculated analytically^{87,88} and 60 trajectories were computed.

In all cases, the selection of initial configurations was made by creating the harmonic-oscillator Wigner distribution (0 K) around the ground state minimum and then considering the computed transition probabilities for each point in the ensemble, as discussed in Ref. 89. For the TDDFT dynamics, initial conditions were sampled in restricted energy windows. The definition of these spectral windows, the number of trajectories initiated in each window, and the initially excited states will be discussed later. MRCIS trajectories were initiated in the restricted spectral window 6.4 ± 0.5 eV, which is centered at the calculated band maximum.

RI-CC2 and most of TDDFT calculations were performed with the TURBOMOLE program.⁸⁰ TDDFT calculations and dynamics simulations using the CAM-B3LYP and the M06-HF functionals were carried out with GAUSSIAN 09.⁹⁰ CASPT2 calculations were performed with the MOLCAS program.⁹¹ For *ab initio* MRCIS calculations, the COLUMBUS program was used.^{92–94} TDDFT and MRCIS surface-hopping dynamics simulations were performed with the NEWTON-X program^{95,96} interfaced with TURBOMOLE and COLUMBUS, respectively. A development version of the MNDO package was employed to calculate the excited state potential energy curves and dynamics with the OM2/MRCI level.^{69,71}

The puckering of the six-membered pyrimidine ring of adenine at conical intersections, stationary points, and geometries visited during the dynamics was characterized

TABLE II. Vertical excitation energies (in eV) at TDDFT level using different functionals. Oscillator strengths in parenthesis. The experimental value for the π - $\pi^*(L_a)$ state is 5.16 ± 0.07 eV. The amount of HF exchange in the functional increases from left (0% in PBE) to right (100% in M06-HF).

	TDDFT/SVP-aug					
	PBE 0%	B3LYP 20%	PBE0 25%	CAM-B3LYP 19%–65%	BHLYP 50%	M06-HF 100%
n - π^*	4.14 (0.000)	4.88 (0.002)	5.02 (0.001)	5.30 (0.007)	5.76 (0.000)	4.90 (0.000)
π - $\pi^*(L_a)$	4.51 (0.130)	5.04 (0.205)	5.16 (0.234)	5.37 (0.287)	5.58 (0.309)	5.06 (0.230)
π - $\pi^*(L_b)$	4.92 (0.054)	5.29 (0.045)	5.41 (0.044)	5.49 (0.013)	5.78 (0.020)	5.32 (0.036)
π -3s(N9)	5.13 (0.006)	5.58 (0.008)	5.82 (0.008)	6.02 (0.010)	6.05 (0.008)	5.01 (0.003)
π -3s(NH ₂)	5.50 (0.004)	5.94 (0.004)	6.20 (0.002)	6.19 (0.001)	6.49 (0.002)	5.45 (0.001)
n - π^*	4.88 (0.001)	5.52 (0.001)	5.66 (0.001)	5.88 (0.002)	6.30 (0.003)	5.53 (0.002)

in a quantitative manner by computing the Cremer-Pople parameters (Q , θ , and ϕ).⁹⁷ Q describes the degree of puckering. The other two parameters, θ and ϕ , describe the type of ring puckering and the atoms involved in it. Every point in the θ - ϕ space can be conveniently classified in terms of the ring conformations as proposed by Boeyens.⁹⁸

III. RESULTS AND DISCUSSION

A. Vertical excitations

The low energy region of the UV spectrum of adenine is characterized by three states: a dark n - π^* , a weakly absorbing π - $\pi^*(L_b)$ and a strongly absorbing π - $\pi^*(L_a)$ state, as shown in Tables II and III. These three states lie close together and their order in the Franck-Condon region is rather dependent on the theoretical method (Fig. 2). Recently, based on experimental results and theoretical corrections for the shift between the band peak and the vertical excitation, Barbatti and Ullrich have proposed that the reference value for the experimental vertical excitation into the π - $\pi^*(L_a)$ state is 5.16 ± 0.07 eV.⁹⁹ The collection of TDDFT results in Table II shows that the best agreement is found for the PBE0 functional (5.16 eV). Functionals with lower Hartree-Fock (HF) exchange contributions tend to underestimate this energy, while those with higher HF exchange contributions (with the exception of the M06-HF) tend to overestimate it. Similar trends can also be observed for the n - π^* and π - $\pi^*(L_b)$ states. Taken together, in the sequence from 0% to 100% of HF exchange included by the PBE (0%), B3LYP (20%), PBE0 (25%), BHLYP (50%), and M06-HF (100%) functionals, the energy gap between

the π - $\pi^*(L_a)$ and n - π^* states tends to decrease until it becomes negative [π - $\pi^*(L_a)$ below n - π^*] for BHLYP and positive again for M06-HF (see Fig. 2). CAM-B3LYP, whose fraction of HF exchange varies between 19% and 65% depending on r_{12} ,⁶⁴ yields a value between PBE0 and BHLYP.

The vertical excitation energies predicted for the π - $\pi^*(L_a)$ state by the MS-CASPT2, RI-CC2, and DFT/MRCI methods are in very good agreement with the experimental result (Table III). Unfortunately, none of these methods can be employed for dynamics simulations, either due to the high computational costs (MS-CASPT2) or because of the lack of analytical energy gradients (DFT/MRCI) and nonadiabatic couplings (all of them). Instead, dynamics has been performed with faster methods such as the *ab initio* MRCIS or the semi-empirical OM2/MRCI method. The *ab initio* MRCIS calculations strongly overestimate the π - $\pi^*(L_a)$ energy (by 1.3–1.5 eV), while OM2/MRCI underestimates it (by 0.5 eV).

B. S₁ minimum, S₁/S₀ conical intersections, and reaction pathways

The minimum of adenine on the S₁ surface has mixed n - π^* and π - π^* character. Geometry optimizations at CASSCF,²⁰ MRCIS, RI-CC2, and OM2/MRCI levels indicate that it is puckered at the C2 atom, usually with a ²E conformation (see Table IV and Fig. 1). The degree of puckering (Q) is about 0.3 Å for the *ab initio* methods and 0.15 Å for OM2/MRCI. In the latter case, the geometry shows also an out-of-plane distortion of C5 not observed in the other methods (²C₅ conformation). All the *ab initio* and semi-empirical

TABLE III. Vertical excitation energies (in eV) at *ab initio* and semi-empirical levels. Oscillator strengths in parenthesis. The experimental value for the π - $\pi^*(L_a)$ state is 5.16 ± 0.07 eV.

	MS-CASPT2		RICC2	MRCIS		DFT/MRCI	OM2/MRCI
	aug-cc-pVDZ ^a	aug-cc-pVTZ ^b	aug-cc-pVDZ	1n ^c	2n ^d	aug-cc-pVDZ	4 or 5 refs ^e
cs	0.00	0.00	0.00	0.00	0.00	0.00	0.00
n - π^*	5.15 (0.002)	5.04 (0.002)	5.08 (0.020)	5.98 (0.001)	6.05 (0.000)	5.13 (0.002)	4.58 (0.00)
π - $\pi^*(L_b)$	5.22 (0.097)	5.02 (0.015)	5.13 (−0.037)	6.23 (0.094)	6.42 (0.059)	5.01 (0.147)	4.97 (0.14)
π - $\pi^*(L_a)$	5.10 (0.130)	5.11 (0.398)	5.16 (0.304)	6.49 (0.250)	6.68 (0.229)	5.08 (0.229)	4.66 (0.21)

^aThis work. SA-5-CASSCF(16,12). Imaginary level shift 0.2 a.u. IPEA = 0.25 a.u.

^bReference 101. π - π^* : CAS(12,13); n - π^* : CAS(18,16). Real level shift 0.3 a.u. IPEA = 0.25 a.u.

^cReference 24. MRCIS(6,4)/SA-4-CASSCF(12,10)/B_{mix} (1n orbital).

^dThis work. MRCIS(6,4)/SA-5-CASSCF(10,8)/6-31G* (2n orbitals).

^eThe results are numerically the same to two decimal digits, regardless of whether 4 or 5 reference configurations are used.

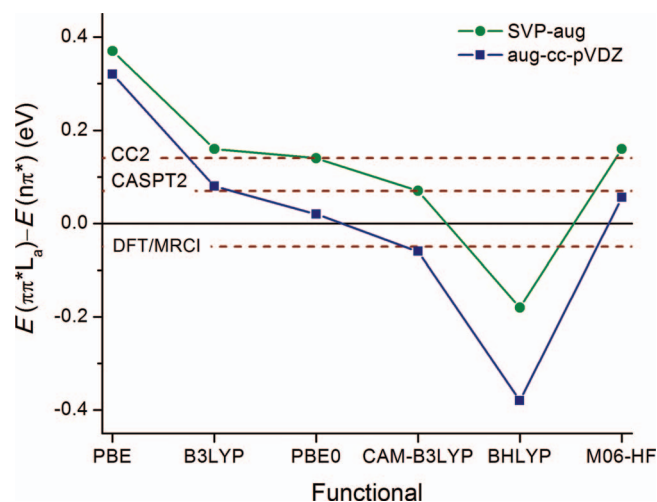


FIG. 2. Energy gap between the $\pi\pi^*(L_a)$ and the $n\pi^*$ states. CC2/aug-cc-pVTZ result from Ref. 100. MS-CASPT2/aug-cc-pVTZ result from Ref. 101.

methods indicate that there is a large degree of mixing between $n\pi^*$ and $\pi-\pi^*$ at this minimum (30%–40% of $\pi-\pi^*$ contribution).

The TDDFT results show a quite different picture: the S_1 minimum is predicted by most of the tested functionals to be planar ($Q = 0 \text{ \AA}$) and to have pure $n\pi^*$ character, without any $\pi-\pi^*$ mixing. Exceptions are the results obtained with TD-BHLYP and TD-M06-HF. In both cases, an appreciable degree of C2 puckering (see Q in Table IV) and state mixing is observed.

The main conical intersections (see Fig. 1) are characterized in Table V. Optimizations at the OM2/MRCI and *ab initio* MRCIS level result in very similar structures for the C2-puckered intersection. The C6-puckered intersection has a larger degree of puckering and some N_1 distortion with

TABLE IV. Characterization of the S_1 minimum of adenine in terms of Q (degree of puckering) and conformation. Percentage of trajectories following the C2-puckered pathway for the M spectral window within 1 ps. HF – fraction of Hartree-Fock exchange in the functional.

Level	HF (%)	Basis set	C2 path (%)	Q (\AA)	Conf.
TD-PBE	0	SVP-aug	0	0.00	Planar
	0	aug-cc-pVDZ	...	0.00	Planar
TD-B3LYP	20	SVP-aug	5	0.00	Planar
	20	aug-cc-pVDZ	...	0.00	Planar
TD-PBE0	25	SVP-aug	0	0.00	Planar
	25	aug-cc-pVDZ	...	0.00	Planar
TD-CAM-B3LYP	19–65	SVP-aug	20	0.00	Planar
	19–65	aug-cc-pVDZ	...	0.00	Planar
TD-BHLYP	50	SVP-aug	25	0.17	2E
	50	aug-cc-pVDZ	...	0.22	2E
TD-M06-HF	100	SVP-aug	0	0.24	2H_3
	100	aug-cc-pVDZ	...	0.30	2E
CASSCF ^a		6-31G*		0.29	2E
MRCIS-1n		B_{mix}	80	0.38	2E
MRCIS-2n		6-31G*	74	0.34	2E
OM2/MRCI		OM2	7	0.15	2C_5
RI-CC2		aug-cc-pVDZ	...	0.26	2E

^aSA2-CASSCF(12,10), Ref. 20.

TABLE V. Geometrical characterization of the C2- and C6-puckered conical intersections of 9H-adenine optimized at OM2/CI (5 references) and *ab initio* MRCIS-2n levels. d_{MW} is the mass-weighted distance between the conical intersection and the ground state minimum geometries. The values in parenthesis are MRCIS-1n results from Ref. 24. Q , θ , and ϕ are the Cremer-Pople parameters.

	C2-puckered		C6-puckered	
	OM2/CI	MRCIS	OM2/CI	MRCIS
ΔE (eV)	4.12	4.75 (4.61)	3.91	4.99 (5.29)
d_{MW} ($\text{\AA} \text{ amu}^{1/2}$)	3.44	3.39 (3.21)	6.99	6.19 (5.87)
Q (\AA)	0.548	0.542 (0.537)	0.351	0.455 (0.463)
θ ($^\circ$)	65.1	69.0 (68.7)	138.9	122.7 (124.6)
ϕ ($^\circ$)	71.4	66.3 (68.4)	117.5	151.1 (161.9)
Conformation	E_2	E_2 (E_2)	6E	6H_1 (6H_1)

MRCIS. For the C2- and C6-puckered conical intersections, OM2/MRCI predicts lower energies than MRCIS, with an especially pronounced deviation in the case of the C6-puckered conical intersection.

The potential energy profiles on the pathways between the ground state minimum geometry and the C2- and C6-puckered conical intersection geometries are shown for several methods in Fig. 3. The energies are also tabulated in the supplemental material.⁵⁸ These pathways were built by linear interpolation in natural internal coordinates¹⁰² between these geometries. In the case of the OM2/MRCI and *ab initio* MRCIS pathways, the conical intersection geometries were optimized at same level as employed in the pathway calculation. For the TDDFT pathways, the MRCIS conical intersection geometries were relaxed on the S_1 surface at the TDDFT level until a minimum energy gap with the ground state was found. In these cases, the geometries at the end of the pathways are not strictly a conical intersection. The same procedure was employed to build the RI-CC2 pathways. For the CASPT2 and DFT/MRCI pathways, the MRCIS and PBE0 geometries were employed, respectively.

At the ground state minimum ($0 \text{ \AA} \text{ amu}^{1/2}$), the OM2/MRCI and the RI-CC2 profiles show a slope towards the C6-puckered side. On the other hand, the MRCIS and DFT/MRCI profiles show an opposite slope towards the C2-puckered side. The CASPT2 and TDDFT pathways do not show any clear trend towards either side.

The SS-CASPT2 energy profile is not smooth because of the change of character of the states along the path. This is fixed by the MS-CASPT2 procedure. Near the conical intersections, however, SS-CASPT2 predicts energy crossings, while MS-CASPT2 yields large energy gaps. This is an indication that the state interaction is too large in the MS procedure, implying that the current active space is still too small to describe the crossing regions.¹⁰³

As discussed in the Introduction, experimental measurements yield two time constants around 0.1 ps and 1 ps.¹⁶ The short time constant is associated to multiphoton processes near zero pump-probe delay time and to the relaxation of adenine to the S_1 surface. For this reason, the reaction pathways between the S_1 minimum and the conical intersections may be more significant than the pathways between the Franck-Condon region and the intersections. Figure 4 shows the

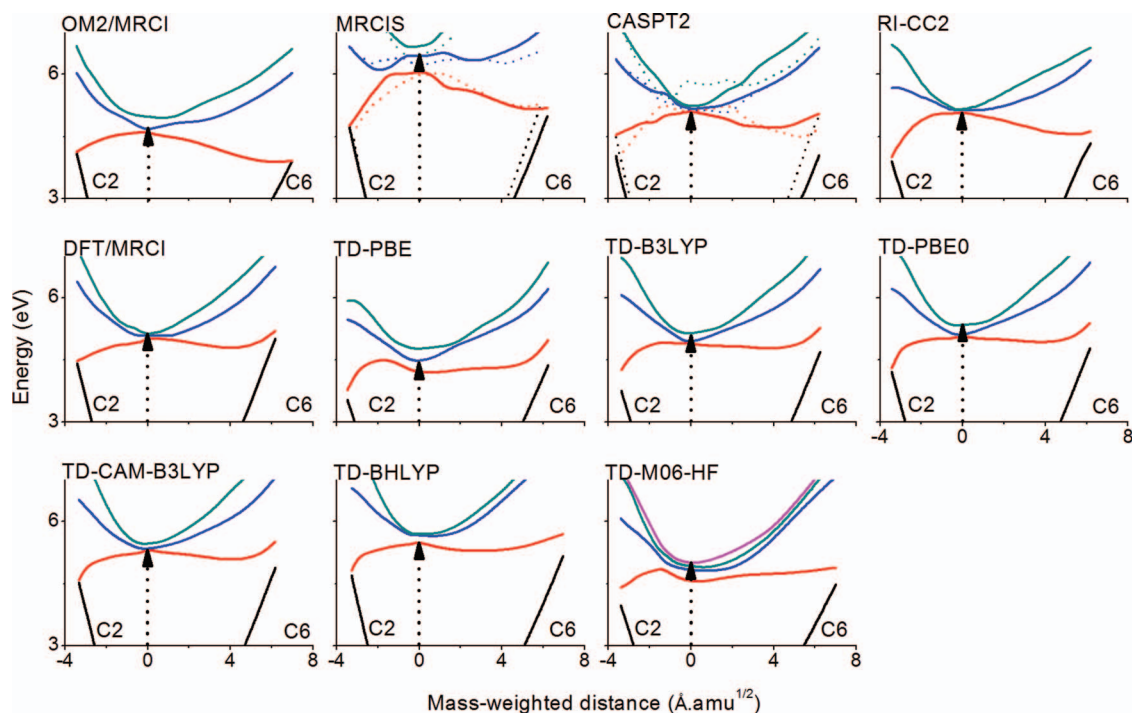


FIG. 3. Potential energy profiles for reaction pathways between the ground state minimum geometry ($0 \text{ \AA amu}^{1/2}$) and the conical intersections puckered at C6 and C2 for different theoretical levels. Ground state energies are only partially shown (near the end of the pathways). TDDFT, RI-CC2, and DFT/MRCI with aug-cc-pVDZ. CASPT2: SS–dotted lines; MS–solid lines. MRCIS: 1n–dotted lines; 2n–solid lines.

energy profiles for the linearly interpolated pathways between the S_1 minimum and the C2- and C6-puckered conical intersections computed with different methods. The energies are also tabulated in the supplemental material.⁵⁸ Note that all energy barriers in Fig. 4 will be overestimated due to the linear interpolation procedure. These barriers have been discussed

more properly in Refs. 20 and 21, where the reaction pathways were obtained by minimum energy path computation.

The pathways in Fig. 4 show that, starting from the S_1 minimum, adenine can access both conical intersections by overcoming potential energy barriers. The barrier heights vary with the method, but in general they are lower for the

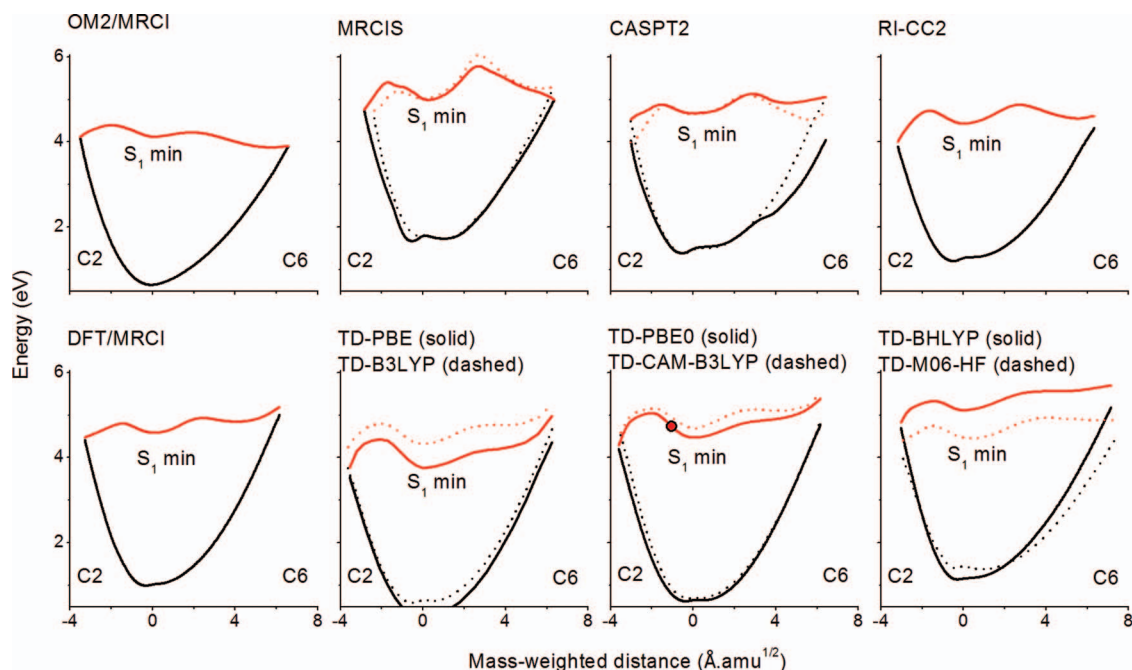


FIG. 4. Potential energy profiles for reaction pathways between the S_1 minimum geometry ($0 \text{ \AA amu}^{1/2}$) and the conical intersections puckered at C6 and C2 for different theoretical levels. TDDFT and RI-CC2 with aug-cc-pVDZ. CASPT2: SS–dashed lines; MS–solid lines. MRCIS: 1n–dashed lines; 2n–solid lines. The circle in the TD-PBE0 profile indicates the peak of the Q distribution during the dynamics simulations.

pathway towards C2 than C6 puckering. Exceptions to this pattern are the OM2/MRCI and the TD-PBE0 profiles. In particular, taking into account that the barriers will be overestimated, the OM2/MRCI barrier to C6 puckering is negligible. On the other hand, it is clear from the comparisons with the CASPT2 and CC2 results that MRCIS overestimates the barrier to C6 puckering.

C. Dynamics at *ab initio* and semi-empirical MRCI levels

Dynamics simulations at the OM2/MRCI and *ab initio* MRCIS levels for adenine in the gas phase predict fast sub-picosecond decay (Table VI). At MRCIS-1n, the fraction of trajectories converted to the ground state within 1 ps is about 15% larger than the experimental result for all three spectral windows. This overestimation reaches 25% for MRCIS-2n. For both levels, it reflects the too large initial energies predicted by MRCIS (Table III), which speeds up the dynamics. Using OM2/MRCI without decoherence correction, the excited state lifetime is also too short and the fraction of trajectories converted to the ground state within 1 ps [83% (79%) with 4 (5) reference configurations] is somewhat larger than the experimental result of 70% (Table VI). When the decoherence correction is applied, the lifetime increases (Table I) and the fraction of trajectories converted to the ground state drops to 59%. Even though MRCIS and OM2/MRCI present similar deactivation rates, different dominant deactivation pathways are found with these methods as shown in Table I.

The divergence can be better visualized if we compare the kind of ring puckering accessed by the *ab initio* and semi-empirical dynamics, as done in Fig. 5. This figure shows the distribution of trajectories in the Cremer-Pople space θ - ϕ . Each point in this space corresponds to a different kind of

TABLE VI. Fraction of the population converted to the ground state after 1 ps according to experiments and simulations at several theoretical levels. Gas-phase data supposing single exponential decay, as a function of the initial excitation energy.

	Initial energy window			Full
	Low	Medium	High	
MRCIS-1n ^a	73	80	90	84
MRCIS-2n	...	85
OM2/MRCI (4 refs) ^b	83
OM2/MRCI (5 refs) ^c	79
OM2/MRCI (5 refs) ^d	59
TD-B3LYP	0	20	20	...
TD-PBE0	0	0	18	...
TD-PBE	...	5
TD-BHLYP	...	25
TD-CAM-B3LYP	...	20
TD-M06-HF	...	10
Expt. ^e	62	68	75	~70

^aReferences 11 and 24.

^bReference 9.

^cWithout decoherence correction.

^dWith decoherence correction.

^eExperimental data according to the lifetimes provided for 265.1 nm (L), 251.3 nm (M), and 238.1 nm (H) pump wavelengths in Ref. 55.

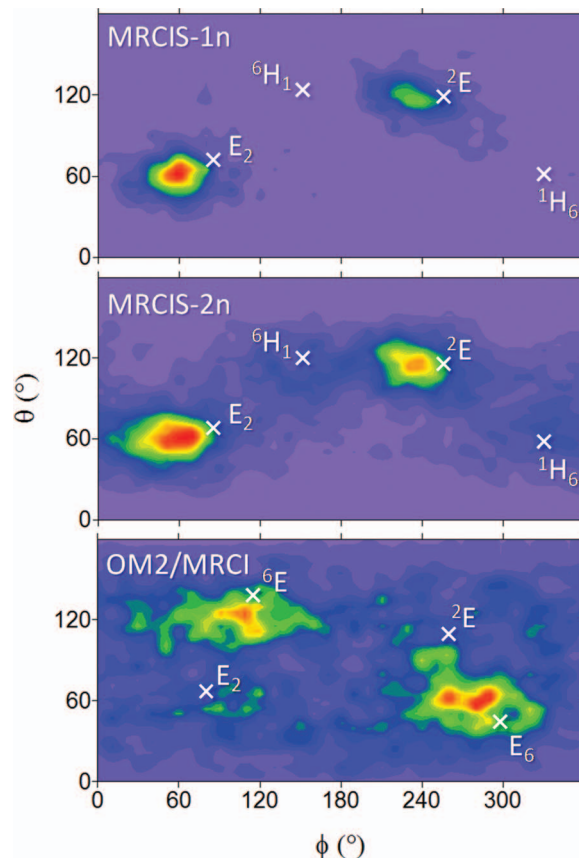


FIG. 5. Distribution of the Cremer-Pople parameters θ and ϕ for trajectories simulated with MRCIS-1n, MRCIS-2n, and OM2/MRCI (5 references, no decoherence correction). MRCIS-1n data from Ref. 24. The crosses indicate the conical intersections computed at each level. Red regions are more densely populated.

pyrimidine ring puckering (see the supplemental material⁵⁸ for more information on the Cremer-Pople-Boeyens analysis). From all trajectories, all time steps before the hopping to the ground state were included in the distribution. While at the *ab initio* level, the pyrimidine ring is puckered exclusively (MRCIS-1n) or mostly (MRCIS-2n) at the C2 atom during the excited state dynamics, a broader distribution of ring puckering types is observed for OM2/MRCI, with the maxima of the distribution around C6-puckered conformations.

The present MRCIS-2n results were computed using a similar approach as before,²⁴ but including two pyrimidine n orbitals in the CAS space (as opposed to only one in the previous MRCIS-1n study) and using an improved basis set. Besides that, a more statistically significant number of trajectories are computed in the present work (60 trajectories in the middle energy window against 60 trajectories over the whole spectrum in Ref. 24). Although the results from both sets of MRCIS calculations are similar, the present calculations introduce a new element not observed before. While dynamics based on a CAS containing only one n orbital shows exclusively ring puckering at the C2 atom (Fig. 5, top), dynamics based on a CAS space containing two n orbitals shows ring puckering at the C6 atom as well (Fig. 5, middle), although with a small probability. This result is consistent with the analysis of Ref. 104, which showed similar effect in the

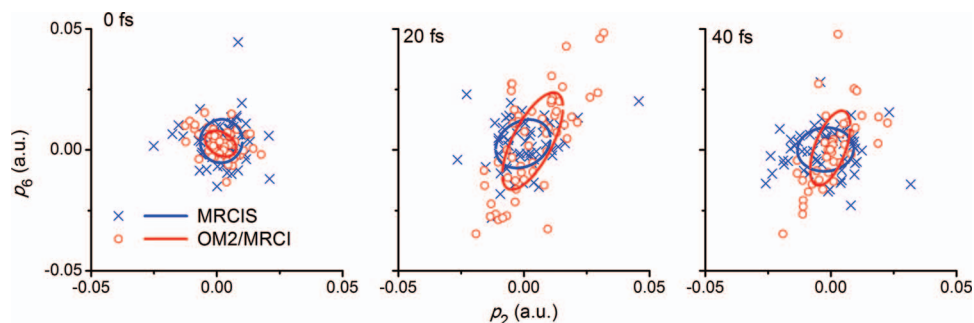


FIG. 6. Gradient projection along the C2 and C6 puckering directions for 60 trajectories simulated with OM2/MRCI (5 references, no decoherence correction) and *ab initio* MRCIS methods at times 0, 20, and 40 fs. The elliptical fitting of data is shown as well.

dynamics of aminopyrimidine performed with different active spaces. In that work, it was shown that while an active space containing only one n orbital did not show any deactivation through C6-puckering, an active space containing two n orbitals showed 15% of deactivation through this channel.

A first hint into the source of the divergence between OM2/MRCI and *ab initio* MRCIS is already given by the reaction pathways plotted in Fig. 4. The S_1 state shows a clear trend towards C2 puckering for MRCIS and towards C6 puckering for OM2/MRCI. To check the hypothesis that the topography of the potential energy surfaces at the beginning of the dynamics determines the further dynamical behavior, we have investigated the initial evolution of both sets of simulations. This was done by computing the projection of the energy gradient towards the conical intersections for each trajectory at certain time steps, as explained in the supplemental material.⁵⁸ The results of this procedure are shown in Fig. 6. Initially, at time 0, the gradient-projection distribution is equivalent for both methods, which implies that the initial conditions for each method are not responsible for the different results. As soon as 20 fs later, the OM2/MRCI results show already a clear trend towards the C6-puckering direction, while the MRCIS results are still almost isotropic.

The analysis of the trajectories shows that the OM2/MRCI dynamics relaxes to the C2-puckered S_1 minimum but quickly moves towards C6-puckered structures because this motion is overly favored by the S_1 potential energy profile, which has a negligible barrier in this direction (see Fig. 4). This creates a bias favoring deactivation via the C6-puckered conical intersections. This scenario is basically the same for all three sets of OM2/MRCI trajectories (Table VI).

The MRCIS dynamics also proceeds first by relaxing to the C2-puckered S_1 minimum (Table IV and Fig. 1). From this S_1 minimum, MRCIS trajectories face an artificially large barrier to follow the C6 pathway (compared with CASPT2 and RI-CC2) and a much smaller barrier to follow the C2 pathway (see Fig. 4). This imbalance between the barriers towards the C2 and C6 pathways creates a bias favoring deactivation via C2-puckered conical intersections.

This analysis makes clear that the discrepancies between the semi-empirical OM2/MRCI and *ab initio* MRCIS results are due to two factors: first, the too strong stabilization of the C6 pathway at the OM2/MRCI level inducing different initial dynamics and, second, the imbalance between the barriers to

escape from the S_1 minimum at the *ab initio* MRCIS level, blocking the C6 pathway.

Taking the CASPT2 results as the reference level, the energy profiles for the reaction pathways between the S_1 minimum and the conical intersections (Fig. 4) indicate that the real dynamics should still be dominated by the C2 pathway, but substantial participation of the C6 pathway in the internal conversion may be expected as well. In this sense, the inclusion of a second n orbital in the reference space of the MRCIS-2n simulations has helped to get a more balanced picture of the reaction pathway, with some degree of deactivation via the C6 pathway. However, the present MRCIS-2n results can still not be considered definitive because of the inherent limitations in the chosen one-electron basis (6-31G*) and correlation treatment (size of the active space, CIS with a limited number of reference configurations), which are reflected in excessively high Franck-Condon energies (see Table III). In this context, we also note that there were frequent orbital rotations in the CI space causing discontinuities along the potential energy surfaces during the *ab initio* MRCIS dynamics.

D. Dynamics at TDDFT levels

TDDFT is one of the most computationally efficient first-principles methods for excited state calculations. Nevertheless, even though it may predict good vertical excitations, it suffers from a series of deficiencies, which may jeopardize dynamics simulations. First, TDDFT is a single-reference method, making it obviously inadequate to describe regions of multireference character,¹⁰⁵ such as conical intersections with the ground state. Conical intersections between excited states, however, may still be handled provided that the involved states can be described as single excitations from a common reference. Second, the linear-response approximation usually employed in the time-dependent procedure cannot properly treat double excitations, which may occur in the course of the dynamics.¹⁰⁶ Third, conventional functionals often fail to describe delocalized states, especially those with charge transfer character, which may also pose serious problems in dynamics simulations.¹⁰⁷ These can be alleviated, to some extent, by the use of long-range corrected functionals,¹⁰⁸ but the efficacy of these functionals for excited state dynamics simulations is still to be evaluated. In the recent literature, there are several reports of successful excited state nonadiabatic dynamics simulations employing TDDFT.^{44,85,109–111}

We have performed dynamics simulations of adenine at the TDDFT level using six popular functionals. The results are not compatible with the experimental data. They are qualitatively wrong for each of the functionals tested. These are bad news for a method whose computational efficiency makes it one of the few allowing the investigation of relatively large systems. The failure of TDDFT to describe adenine dynamics is not entirely surprising given that, as discussed in Sec. III B, most of tested functionals cannot even describe the S_1 minimum properly. In this section, we report these negative results, to gain insight into their origin and to illustrate some limitations of TDDFT.

Surface-hopping dynamics was performed using a sequence of functionals with increasing fraction of HF exchange: PBE (0%), B3LYP (20%), PBE0 (25%), and BHLYP (50%). Complementary adiabatic dynamics simulations on the first excited state were carried out with the M06-HF and the long-range corrected CAM-B3LYP functionals. For the surface-hopping runs, initial conditions were selected from the energy windows indicated in Fig. 7. Initial conditions for TD-B3LYP and TD-PBE0 dynamics were sampled in three energy windows, i.e., in the low (L), medium (M), and high (H) energy regions of the first spectral band. For all other functionals, initial conditions were sampled at medium (M) energies near the band maximum. The definition of the energy windows and a summary of the TDDFT dynamics results are given in Tables VII and VIII.

1. TDDFT dynamics results: B3LYP and PBE0

The first three sets of trajectories were computed using the B3LYP functional. Twenty trajectories were initiated in each energy window, with the distribution of initial states following the contribution of the state to the absorption spectrum.⁸⁵ For instance, in the low-energy window (L), states S_1 and S_2 contribute equally to the absorption spectrum, therefore, an equal number of trajectories (10) were initiated in each of these states.

In the L window, none of the 20 trajectories computed with B3LYP returned to the ground state within 1 ps. By contrast, after excitation near the L window, the experimentally measured lifetime of adenine is $\tau = 1.03$ ps.⁵⁵ Therefore, the ground state population after 1 ps can be estimated as $1 - \exp(-1/\tau)$, or 62%. In the M window, the situation is not much better. From the 20 trajectories started in S_2 , only 4 returned to the ground state within 1 ps, giving a ground state population of 20%, while the experiment indicates a value of 68%. In the H window, also 4 trajectories out of 20 returned to the ground state. Again, the theoretical prediction, 20%, is much below the experimental estimate, 75%. Due to the small number of trajectories computed in each window, these computational results, as well as those for the other functionals below, carry large statistical uncertainties. Nevertheless, the deviations from the experimental results are much too large to be attributed to statistical errors.

The analysis of the TD-B3LYP trajectories shows that they quickly move to the minimum of the S_1 state. Since the internal conversion via a puckered conical intersection

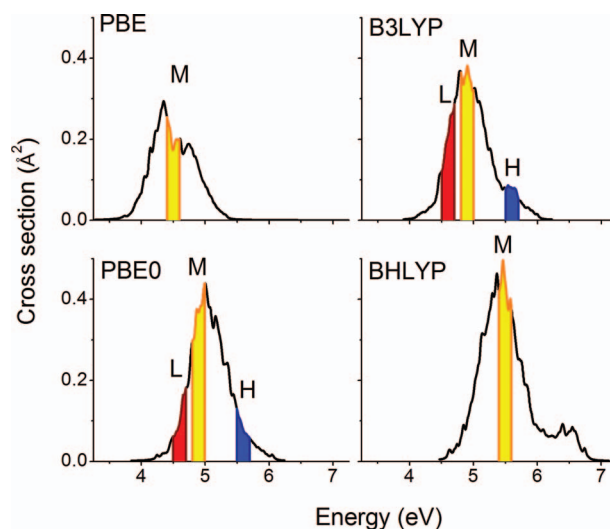


FIG. 7. Absorption cross section computed with TDDFT employing four different functionals. The shaded areas indicated the energy windows (L = low, M = medium, H = high) from which initial conditions were selected for dynamics simulations.

should occur through a crossing between the π - π^* state and the closed-shell ground state, the lack of internal conversion could indicate that TD-B3LYP overestimates the relative stability of the n - π^* state, thus preventing the recrossing to the π - π^* state. This is in line with the computed vertical excitation energies (Table II) and with the finding that the S_1 minimum at this level is planar, has n - π^* character, and does not mix with π - π^* configurations.

Three sets of trajectories were computed with the PBE0 functional. They were initiated in the energy windows shown in Fig. 7, with the distribution of initial states following their contribution to the absorption spectrum. The results of the dynamics simulations are not better than those with B3LYP (within the statistical error). Deactivation is observed neither among the 14 trajectories initiated in the L window nor among the 25 trajectories initiated in the M window (Table VII). Among the 17 trajectories initiated in the H window, 18% return to the ground state within 1 ps.

The results from the B3LYP and PBE0 functionals indicate a much longer lifetime than experimentally observed. We note that previous TDDFTB simulations¹⁰ gave a lifetime of 11 ps for gas-phase adenine, which was attributed to the dependence of the lifetime on the initial conditions. We see here, however, that, even with a well-controlled selection of initial conditions, TDDFT still predicts qualitatively wrong results, and it seems likely that TDDFTB behaves analogously.

Overall, we have observed 11 crossing events to the ground state in these 116 simulations. Except for two of them, which occurred at the C2-puckered conical intersection (Table VII), all others took place at the N9-H stretching conical intersection.

In spite of these disappointing results, there are still some interesting features in these dynamics runs. As previously proposed,^{55,57} the deactivation along the π - σ^* pathway (N9-H dissociation) should occur only above a certain energy threshold. This is confirmed in the simulations. No deactivation is observed in the L window. In the M window

TABLE VII. Number of trajectories (N_{traj}) initiated in each state for TD-B3LYP and TD-PBE0 for each of the three spectral windows. Number of $S_1 \rightarrow S_0$ events and corresponding times (τ_{hop} given in parenthesis). With the exception of the $S_1 \rightarrow S_0$ events marked with “b,” all others correspond to N9-H dissociation.

Initial energy (eV)	B3LYP		PBE0		Exp. ^c
	Initial state (N_{traj})	$N_{S_1 \rightarrow S_0}$ (τ_{hop} , fs)	Initial state (N_{traj})	$N_{S_1 \rightarrow S_0}$ (τ_{hop} , fs)	
4.6 ± 0.1 (L)	S ₁ (10)	0	S ₁ (9)	0	
	S ₂ (10)	0	S ₂ (5)	0	
S ₀ population ^a		0%		0%	62%
4.9 ± 0.1 (M)	S ₂ (20)	4 (45,50, 700 ^b ,900)	S ₁ (7)	0	
			S ₂ (18)	0	
S ₀ population ^a		20%		0%	68%
5.6 ± 0.1 (H)	S ₅ (6)	2 (40,250 ^b)	S ₄ (8)	1 (60)	
	S ₆ (14)	2 (120,120)	S ₅ (9)	2 (45,100)	
S ₀ population ^a		20%		18%	75%

^aS₀ population at 1000 fs.

^bE₂ CI.

^cExperimental data according to the lifetimes provided for 265.1 nm (L), 251.3 nm (M), and 238.1 nm (H) pump wavelengths in Ref. 55.

deactivation is found only for B3LYP, for which the π -3s state (the gateway to the π - σ^* state) lies lower in energy than for PBE0 (see Table II). Deactivation in the H window occurs for both functionals.

2. TDDFT dynamics results: PBE and BHLYP

We now consider the TDDFT dynamics at the limits of having no HF exchange (PBE functional) and a high fraction of HF exchange (50%, BHLYP functional). These results are summarized in Table VIII. In both cases, initial conditions were sampled only in the M window. With PBE, 12 trajectories were started in the S₁ state, while 8 were started in the S₂ state. The ground state population after 1 ps was 5% due to one single trajectory that returned to the ground state via the NH-stretching pathway. This result is, once more, far from the 68% experimentally observed.

With BHLYP, 11 trajectories were started in the S₁ state while 9 were started in the S₂ state. After 1 ps, the ground state population was 25%, the highest deactivation level obtained among all tested functionals. Although this value is still much lower than the experimental result, it is in line with the hypothesis that the description of the n - π^* state may explain why TDDFT performs so badly for adenine. (BHLYP correctly predicts the puckering of the S₁ minimum.) The deactivation occurred exclusively through the C2-puckering pathway in all 5 trajectories that return to the ground state.

3. TDDFT dynamics results: CAM-B3LYP and M06-HF

The slight improvement of the results with a larger fraction of HF exchange in the functional prompted us to test two other functionals, the CAM-B3LYP functional with long-range corrected HF exchange and the M06-HF functional with 100% HF exchange. For both cases, the current implementation of NEWTON-X cannot compute nonadiabatic couplings. Therefore, we ran purely adiabatic dynamics in the S₁ state for a maximum of 1 ps. Ten trajectories were computed for

each functional. The results are compiled in Table VIII. Two TD-CAM-B3LYP trajectories found a C2-puckered crossing with the S₀ state, while the others ended without reaching the crossing seam. In the case of M06-HF, only one trajectory found a crossing with S₀ but along the NH stretching pathway. Once more, there was much less deactivation within 1 ps than experimentally observed, with no sensible improvement over the previous TDDFT results.

TABLE VIII. Number of trajectories (N_{traj}) initiated in each state for TD-PBE, TD-BHLYP, TD-CAM-B3LYP, and TD-M06-HF. Number of $S_1 \rightarrow S_0$ events and corresponding approximate times (τ_{hop} given in parenthesis). With the exception of the $S_1 \rightarrow S_0$ events marked with “b,” all others correspond to N9-H dissociation.

Initial energy (eV)	PBE		Exp. ^c
	Initial state (N_{traj})	$N_{S_1 \rightarrow S_0}$ (τ_{hop} , fs)	
4.5 ± 0.1 (M)	S ₁ (12)	0	
	S ₂ (8)	1 (100 fs)	
S ₀ population ^a		5%	68%
BHLYP			
Initial energy (eV)	Initial state (N_{traj})	$N_{S_1 \rightarrow S_0}$ (τ_{hop} , fs)	Exp. ^c
5.5 ± 0.1 (M)	S ₁ (11)	2 (300 ^b ,600 ^b)	
	S ₂ (9)	3 (700 ^b , 800 ^b , 1000 ^b)	
S ₀ population ^a		25%	68%
CAM-B3LYP			
Initial energy (eV)	Initial state (N_{traj})	$N_{S_1 \rightarrow S_0}$ (τ_{hop} , fs)	Exp. ^c
5.1 ± 0.1 (L)	S ₁ (10)	2 (950 ^b ,860 ^b)	
		20%	
S ₀ population ^a		20%	62%
M06-HF			
Initial energy (eV)	Initial State (N_{traj})	$N_{S_1 \rightarrow S_0}$ (τ_{hop} , fs)	Exp. ^c
4.8 ± 0.1 (L)	S ₁ (10)	2 (90)	
S ₀ population ^a		10%	62%

^aS₀ population at 1000 fs.

^bE₂ CI.

^cExperimental data according to the lifetimes provided for 251.3 nm (M) pump wavelengths in Ref. 55.

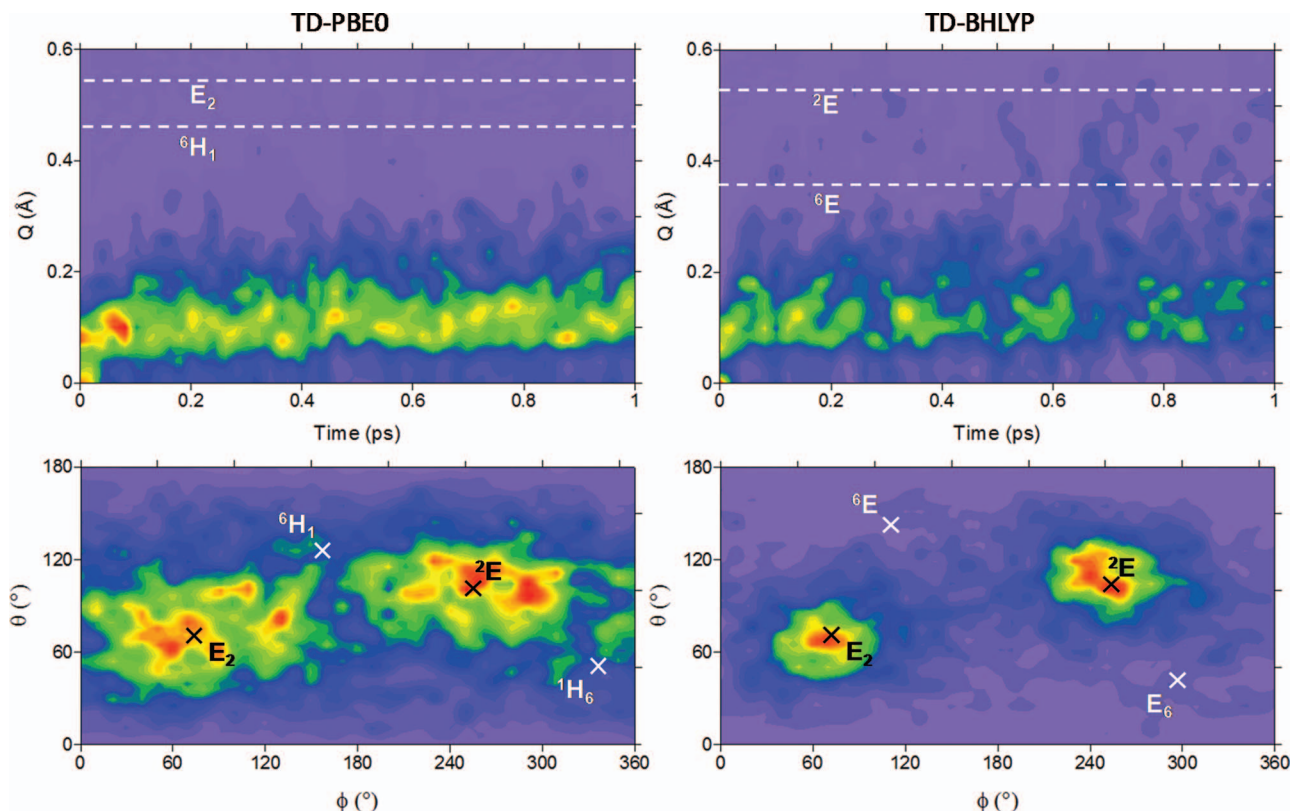


FIG. 8. Cremer-Pople parameters for the M window from the TD-PBE0 and TD-BHLYP dynamics. (Top) Degree of puckering (Q) as a function of time. (Bottom) Type of puckering in terms of ϕ and θ parameters. The parameter values for the last point in the respective reaction pathways, Fig. 4, are indicated by crosses and dashed lines. Red regions are more densely populated.

4. Analysis of the TDDFT trajectories

Figure 8 presents a detailed analysis of the PBE0 results in terms of the Cremer-Pople parameters for the pyrimidine ring. It includes all geometries of all trajectories of the M window. Figure 8 (top left) shows the distribution of the Q parameter as a function of time, while Fig. 8 (bottom-left) shows the distribution of the θ and ϕ parameters for all times. Each point in the θ - ϕ space corresponds to a different kind of ring puckering and the position of the conical intersections is indicated by crosses. Evidently, the pyrimidine ring tends to be puckered during the dynamics. The puckering conformations are broadly distributed in the θ - ϕ space, spanning conformations from E_3 to E_1 . It is particularly relevant that this distribution is centered at E_2 and holds only small contributions from C6-puckered conformations. Figure 8 (top left) shows that the degree of puckering is small, clustered around $Q = 0.1$ Å. As for comparison, the degree of puckering at the conical intersections is above $Q = 0.4$ Å. An analogous analysis for the PBE and B3LYP functionals (not shown) arrives at a similar scenario: adenine tends to pucker at C2, but the degree of puckering is far from what is necessary to reach the C2-puckered conical intersection.

This situation can be rationalized by noting that during the TDDFT dynamics, adenine relaxes to a planar S_1 minimum with strong $n-\pi^*$ character. The oscillation around this minimum along the pyrimidine out-of-plane coordinates creates a distribution peaked at slighted puckered conformations (see Fig. 8). The TD-PBE0 energy profile for the reaction

pathway connecting this planar S_1 minimum to the conical intersections is plotted in Fig. 4 for the PBE0 functional. The peak of Q distribution in Fig. 8 (top left) is marked as a circle in the S_1 curve in Fig. 4. It is obvious from this figure that to move from the S_1 minimum to either conical intersection, adenine has to overcome large energy barriers at the TD-PBE0 level. At the top of the barrier between the S_1 minimum and the C2-puckered conical intersection, adenine is already in the E_2 conformation with $Q = 0.26$ Å. Internal conversion will take place only if the puckering distribution moves to Q values above this value.

The Cremer-Pople analysis of the TD-BHLYP results shows a slightly different scenario (Fig. 8 (right)). In this case, there are already some points above the barrier-puckering threshold ($Q = 0.37$ Å in this case), mainly after 0.4 ps. The conformations are also much more localized around the E_2 region than they were for PBE0. This is a consequence of the S_1 minimum geometry at BHLYP level, which is no longer planar as in the other cases but shows some puckering at C2 ($Q = 0.17$ Å, E_2).

5. Why does TDDFT dynamics fail?

We have analyzed in more detail the energy profiles along the planar and puckered pathways computed at the TD-PBE0 and TD-BHLYP level, using the MS-CASPT2 data as reference (see the supplemental material⁵⁸). This analysis shows that both functionals overly favor ground state planar

distortions in comparison to ground state puckering distortions. In the case of PBE0, the excitation energies obtained with the time-dependent procedure along both pathways are in good agreement with the MS-CASPT2 reference data, but they cannot compensate for the ground state over-stabilization of the planar distortion, leading to the artificial planarity of the S_1 minimum. At this planar minimum, the $n-\pi^*$ and $\pi-\pi^*$ states are decoupled, thus reducing the probability of adenine to recross to the $\pi-\pi^*$ state, which is essential for reaching the conical intersection. The analysis for PBE and B3LYP yields similar results.

In the case of BHLYP, the bias towards planar distortions in the ground state is compensated by too large excitation energies, which are overestimated by this functional. Therefore, the relatively good dynamics results of TD-BHLYP are caused by error compensation.

We have not been able to pinpoint the origin of the over-stabilization of the planar pathways over the puckered pathways in the S_1 state, but we have seen that this artifact largely arises from the ground state DFT potentials, and less from the time-dependent procedure. The overestimation of the excitation energy by the BHLYP functional, on the other hand, can be traced back to the reduction of correlation energy caused by the large fraction of HF exchange.

IV. CONCLUSIONS

The comparative analysis of surface-hopping dynamics and potential energy profiles of adenine with several different methods leads to the following conclusions:

- *Ab initio* MRCIS, semi-empirical OM2/MRCI, and TDDFT dynamics with BHLYP and M06-HF functionals show an initial dynamics towards the C2-puckered S_1 minimum, with strongly mixed $n-\pi^*/\pi-\pi^*$ character. TDDFT dynamics with PBE, B3LYP, PBE0, and CAM-B3LYP functionals show an initial dynamics towards a planar S_1 minimum with pure $n-\pi^*$ character.
- From the C2-puckered minimum, *ab initio* MRCIS simulations lead to deactivation mainly near C2-puckered conical intersections. The deactivation rate is about 15%–25% larger than the experimental result and is determined mainly by the time to escape from the C2-puckered minimum. In the OM2/MRCI dynamics, adenine remains for a short period around the C2-puckered minimum and then moves towards the C6-puckered conical intersection where it deactivates; the deactivation rate is about 15% too high (too low) in runs without (with) decoherence correction. TDDFT trajectories are trapped in the S_1 minimum and yield deactivation at a much slower rate than experimentally observed.
- The *ab initio* MRCIS results exhibit some dependence on the active space, although without changing the overall qualitative picture. The inclusion of an additional n orbital in the calculations leads to a small amount of deactivation via the C6-conical intersection. The inclusion of an additional reference configuration

in the OM2/MRCI calculations causes an increase in the lifetime but has no significant effect on the decay mechanisms.

- The quality of the *ab initio* MRCIS, TDDFT, and OM2/MRCI results can be assessed for the relevant excited state reaction pathways by comparison with MS-CASPT2 and RI-CC2 energy profiles. Such analysis indicates that the previous *ab initio* MRCIS-1n results underestimated the role of the C6-puckered conical intersection due to limitations of the active space. The inclusion of an additional n orbital in the active space (MRCIS-2n) leads to a more balanced description of the pathways. OM2/MRCI overestimates the ease of C6-puckering, and hence the role of the C6-puckered conical intersections. The bad performance of TDDFT is related to an over-stabilization of planar distortions over puckered distortions in the ground state, which favors a planar S_1 minimum and prevents $n\pi^*/\pi\pi^*$ mixing near this minimum.
- None of the functionals tested in the TDDFT calculations delivers satisfactory results. There is no improvement upon including long-range corrections (CAM-B3LYP) and no clear trend with regard to the fraction of HF exchange. In the least unsatisfactory case, BHLYP predicts an S_1 minimum with appreciable $n\pi^*/\pi\pi^*$ mixing (like *ab initio* MRCIS, CASPT2, CC2, and OM2/MRCI), which is, however, caused by error compensation.
- At high initial energies, TDDFT predicts some deactivation (still much below the experimentally observed level) mostly through the N9-H dissociation pathway.
- High-quality reaction pathways are obtained with CC2 and DFT/MRCI. Although CC2 cannot be used to describe the crossing with the ground state, it is possible that it may be a good option for nonadiabatic dynamics involving only excited states. Analytical gradients for DFT/MRCI and nonadiabatic couplings for DFT/MRCI and CC2 need to be developed so that these methods can be effectively used in dynamics simulations.

ACKNOWLEDGMENTS

Z.L. thanks for support from the CAS 100 Talent Project, from the National Science Foundation of China (NSFC) (No. 21103213), and from the Director Innovation Foundation of QIBEBT of CAS. This work has been supported by the Austrian Science Fund within the framework of the Special Research Program and F41 Vienna Computational Materials Laboratory (ViCoM). Support was also provided by the Robert A. Welch Foundation under Grant No. D-0005.

¹V. Bonačić-Koutecký and R. Mitrić, *Chem. Rev.* **105**, 11 (2005).

²M. Garavelli, *Theor. Chem. Acc.* **116**, 87 (2006).

³B. G. Levine and T. J. Martínez, *Annu. Rev. Phys. Chem.* **58**, 613 (2007).

⁴F. Plasser, M. Barbatti, A. Aquino, and H. Lischka, *Theor. Chem. Acc.* **131**, 1073 (2012).

⁵A. Migani and M. Olivucci, in *Conical Intersections: Electronic Structure, Dynamics and Spectroscopy*, edited by W. Domcke, D. R. Yarkony, and H. Köppel (World Scientific, Singapore, 2004).

- ⁶F. Santoro, A. Lami, and M. Olivucci, *Theor. Chem. Acc.* **117**, 1061 (2007).
- ⁷R. Send and D. Sundholm, *J. Phys. Chem. A* **111**, 8766 (2007).
- ⁸O. Valsson and C. Filippi, *J. Chem. Theory Comput.* **6**, 1275 (2010).
- ⁹E. Fabiano and W. Thiel, *J. Phys. Chem. A* **112**, 6859 (2008).
- ¹⁰R. Mitrić, U. Werner, M. Wohlgenuth, G. Seifert, and V. Bonačić-Koutecký, *J. Phys. Chem. A* **113**, 12700 (2009).
- ¹¹M. Barbatti, A. J. A. Aquino, J. J. Szyczak, D. Nachtigallová, P. Hobza, and H. Lischka, *Proc. Natl. Acad. Sci. U.S.A.* **107**, 21453 (2010).
- ¹²M. Barbatti, J. J. Szyczak, A. J. A. Aquino, D. Nachtigallová, and H. Lischka, *J. Chem. Phys.* **134**, 014304 (2011).
- ¹³C. E. Crespo-Hernández, B. Cohen, P. M. Hare, and B. Kohler, *Chem. Rev.* **104**, 1977 (2004).
- ¹⁴M. Daniels and W. Hauswirth, *Science* **171**, 675 (1971).
- ¹⁵S. Ullrich, T. Schultz, M. Z. Zgierski, and A. Stolow, *Phys. Chem. Chem. Phys.* **6**, 2796 (2004).
- ¹⁶C. Canuel, M. Mons, F. Piuze, B. Tardivel, I. Dimicoli, and M. Elhanine, *J. Chem. Phys.* **122**, 074316 (2005).
- ¹⁷C. M. Marian, *J. Chem. Phys.* **122**, 104314 (2005).
- ¹⁸S. Matsika, *J. Phys. Chem. A* **109**, 7538 (2005).
- ¹⁹S. Perun, A. L. Sobolewski, and W. Domcke, *J. Am. Chem. Soc.* **127**, 6257 (2005).
- ²⁰L. Blancafort, *J. Am. Chem. Soc.* **128**, 210 (2006).
- ²¹L. Serrano-Andrés, M. Merchán, and A. C. Borin, *Proc. Natl. Acad. Sci. U.S.A.* **103**, 8691 (2006).
- ²²G. Zechmann and M. Barbatti, *J. Phys. Chem. A* **112**, 8273 (2008).
- ²³L. Serrano-Andrés and M. Merchán, *J. Photochem. Photobiol. C* **10**, 21 (2009).
- ²⁴M. Barbatti and H. Lischka, *J. Am. Chem. Soc.* **130**, 6831 (2008).
- ²⁵M. Barbatti, A. J. A. Aquino, J. J. Szyczak, D. Nachtigallová, and H. Lischka, *Phys. Chem. Chem. Phys.* **13**, 6145 (2011).
- ²⁶J. González-Vázquez and L. González, *ChemPhysChem* **11**, 3617 (2010).
- ²⁷D. Nachtigallová, A. J. A. Aquino, J. J. Szyczak, M. Barbatti, P. Hobza, and H. Lischka, *J. Phys. Chem. A* **115**, 5247 (2011).
- ²⁸D. Nachtigallová, T. Zeleny, M. Ruckebauer, T. Müller, M. Barbatti, P. Hobza, and H. Lischka, *J. Am. Chem. Soc.* **132**, 8261 (2010).
- ²⁹N. L. Doltsinis, P. R. L. Markwick, H. Nieber, and H. Langer, in *Radiation Induced Molecular Phenomena in Nucleic Acids*, edited by M. K. Shukla and J. Leszczynski (Springer, Netherlands, 2008), Vol. 5, p. 265.
- ³⁰H. Langer, N. L. Doltsinis, and D. Marx, *ChemPhysChem* **6**, 1734 (2005).
- ³¹H. Langer and N. L. Doltsinis, *Phys. Chem. Chem. Phys.* **6**, 2742 (2004).
- ³²H. Nieber and N. L. Doltsinis, *Chem. Phys.* **347**, 405 (2008).
- ³³G. Groenhof, L. V. Schafer, M. Boggio-Pasqua, M. Goette, H. Grubmüller, and M. A. Robb, *J. Am. Chem. Soc.* **129**, 6812 (2007).
- ³⁴Z. G. Lan, E. Fabiano, and W. Thiel, *ChemPhysChem* **10**, 1225 (2009).
- ³⁵Z. Lan, E. Fabiano, and W. Thiel, *J. Phys. Chem. B* **113**, 3548 (2009).
- ³⁶J. J. Szyczak, M. Barbatti, J. T. Soo Hoo, J. A. Adkins, T. L. Windus, D. Nachtigallová, and H. Lischka, *J. Phys. Chem. A* **113**, 12686 (2009).
- ³⁷A. N. Alexandrova, J. C. Tully, and G. Granucci, *J. Phys. Chem. B* **114**, 12116 (2010).
- ³⁸Z. Lan, Y. Lu, E. Fabiano, and W. Thiel, *ChemPhysChem* **12**, 1989 (2011).
- ³⁹Y. Lu, Z. Lan, and W. Thiel, *Angew. Chem., Int. Ed.* **50**, 6864 (2011).
- ⁴⁰Y. Lu, Z. Lan, and W. Thiel, *J. Comput. Chem.* **33**, 1225 (2012).
- ⁴¹Y. Lei, S. Yuan, Y. Dou, Y. Wang, and Z. Wen, *J. Phys. Chem. A* **112**, 8497 (2008).
- ⁴²H. R. Hudock and T. J. Martínez, *ChemPhysChem* **9**, 2486 (2008).
- ⁴³H. R. Hudock, B. G. Levine, A. L. Thompson, H. Satzger, D. Townsend, N. Gador, S. Ullrich, A. Stolow, and T. J. Martínez, *J. Phys. Chem. A* **111**, 8500 (2007).
- ⁴⁴D. Picconi, V. Barone, A. Lami, F. Santoro, and R. Improta, *ChemPhysChem* **12**, 1957 (2011).
- ⁴⁵F. Santoro, R. Improta, and V. Barone, *Theor. Chem. Acc.* **123**, 273 (2009).
- ⁴⁶R. Improta, V. Barone, A. Lami, and F. Santoro, *J. Phys. Chem. B* **113**, 14491 (2009).
- ⁴⁷R. Improta, F. Santoro, V. Barone, and A. Lami, *J. Phys. Chem. A* **113**, 15346 (2009).
- ⁴⁸D. C. Luhrs, J. Viallon, and I. Fischer, *Phys. Chem. Chem. Phys.* **3**, 1827 (2001).
- ⁴⁹H. Kang, K. T. Lee, B. Jung, Y. J. Ko, and S. K. Kim, *J. Am. Chem. Soc.* **124**, 12958 (2002).
- ⁵⁰H. Kang, B. Jung, and S. K. Kim, *J. Chem. Phys.* **118**, 6717 (2003).
- ⁵¹S. Ullrich, T. Schultz, M. Z. Zgierski, and A. Stolow, *J. Am. Chem. Soc.* **126**, 2262 (2004).
- ⁵²H. Satzger, D. Townsend, M. Z. Zgierski, S. Patchkovskii, S. Ullrich, and A. Stolow, *Proc. Natl. Acad. Sci. U.S.A.* **103**, 10196 (2006).
- ⁵³H. Satzger, D. Townsend, and A. Stolow, *Chem. Phys. Lett.* **430**, 144 (2006).
- ⁵⁴C. H. Chin, A. M. Mebel, G. S. Kim, K. Y. Baek, M. Hayashi, K. K. Liang, and S. H. Lin, *Chem. Phys. Lett.* **445**, 361 (2007).
- ⁵⁵N. L. Evans and S. Ullrich, *J. Phys. Chem. A* **114**, 11225 (2010).
- ⁵⁶B. Cohen, P. M. Hare, and B. Kohler, *J. Am. Chem. Soc.* **125**, 13594 (2003).
- ⁵⁷M. G. D. Nix, A. L. Devine, B. Cronin, and M. N. R. Ashfold, *J. Chem. Phys.* **126**, 124312 (2007).
- ⁵⁸See supplementary material at <http://dx.doi.org/10.1063/1.4731649> for computational details, characteristic energies, analysis of TDDFT pathways, and Cartesian coordinates.
- ⁵⁹J. P. Perdew, M. Ernzerhof, and K. Burke, *J. Chem. Phys.* **105**, 9982 (1996).
- ⁶⁰A. D. Becke, *J. Chem. Phys.* **98**, 5648 (1993).
- ⁶¹P. J. Stephens, F. J. Devlin, C. F. Chabalowski, and M. J. Frisch, *J. Phys. Chem.* **98**, 11623 (1994).
- ⁶²J. P. Perdew, K. Burke, and M. Ernzerhof, *Phys. Rev. Lett.* **77**, 3865 (1996).
- ⁶³A. D. Becke, *J. Chem. Phys.* **98**, 1372 (1993).
- ⁶⁴T. Yanai, D. P. Tew, and N. C. Handy, *Chem. Phys. Lett.* **393**, 51 (2004).
- ⁶⁵Y. Zhao and D. Truhlar, *Theor. Chem. Acc.* **119**, 525 (2008).
- ⁶⁶T. H. Dunning, *J. Chem. Phys.* **90**, 1007 (1989).
- ⁶⁷F. Weigend and R. Ahlrichs, *Phys. Chem. Chem. Phys.* **7**, 3297 (2005).
- ⁶⁸A. Koslowski, M. E. Beck, and W. Thiel, *J. Comput. Chem.* **24**, 714 (2003).
- ⁶⁹W. Weber and W. Thiel, *Theor. Chem. Acc.* **103**, 495 (2000).
- ⁷⁰N. Otte, M. Scholten, and W. Thiel, *J. Phys. Chem. A* **111**, 5751 (2007).
- ⁷¹W. Thiel, MNDO Program, version 6.1, Max-Planck-Institut für Kohlenforschung, Mülheim an der Ruhr, Germany, 2007.
- ⁷²M. R. Silva-Junior and W. Thiel, *J. Chem. Theory Comput.* **6**, 1546 (2010).
- ⁷³O. Christiansen, H. Koch, and P. Jorgensen, *Chem. Phys. Lett.* **243**, 409 (1995).
- ⁷⁴C. Hättig and F. Weigend, *J. Chem. Phys.* **113**, 5154 (2000).
- ⁷⁵C. Hättig and A. Köhn, *J. Chem. Phys.* **117**, 6939 (2002).
- ⁷⁶J. Finley, P. A. Malmqvist, B. O. Roos, and L. Serrano-Andrés, *Chem. Phys. Lett.* **288**, 299 (1998).
- ⁷⁷G. Ghigo, B. O. Roos, and P.-A. Malmqvist, *Chem. Phys. Lett.* **396**, 142 (2004).
- ⁷⁸S. Grimme and M. Waletzke, *J. Chem. Phys.* **111**, 5645 (1999).
- ⁷⁹F. Weigend, M. Häser, H. Patzelt, and R. Ahlrichs, *Chem. Phys. Lett.* **294**, 143 (1998).
- ⁸⁰R. Ahlrichs, M. Bär, M. Häser, H. Horn, and C. Kölmel, *Chem. Phys. Lett.* **162**, 165 (1989).
- ⁸¹W. J. Hehre, R. Ditchfield, and J. A. Pople, *J. Chem. Phys.* **56**, 2257 (1972).
- ⁸²G. Granucci and M. Persico, *J. Chem. Phys.* **126**, 134114 (2007).
- ⁸³J. C. Tully, *J. Chem. Phys.* **93**, 1061 (1990).
- ⁸⁴S. Hammes-Schiffer and J. C. Tully, *J. Chem. Phys.* **101**, 4657 (1994).
- ⁸⁵M. Barbatti, J. Pittner, M. Pederzoli, U. Werner, R. Mitrić, V. Bonačić-Koutecký, and H. Lischka, *Chem. Phys.* **375**, 26 (2010).
- ⁸⁶S. Patchkovskii, A. Koslowski, and W. Thiel, *Theor. Chem. Acc.* **114**, 84 (2005).
- ⁸⁷M. Dallos, H. Lischka, E. V. do Monte, M. Hirsch, and W. Quapp, *J. Comput. Chem.* **23**, 576 (2002).
- ⁸⁸H. Lischka, M. Dallos, and R. Shepard, *Mol. Phys.* **100**, 1647 (2002).
- ⁸⁹M. Barbatti, A. J. A. Aquino, and H. Lischka, *Phys. Chem. Chem. Phys.* **12**, 4959 (2010).
- ⁹⁰M. J. Frisch, G. W. Trucks, H. B. Schlegel *et al.*, GAUSSIAN 09, Revision A.02, Gaussian, Inc., Wallingford, CT, 2009.
- ⁹¹G. Karlström, R. Lindh, P. A. Malmqvist, B. O. Roos, U. Ryde, V. Veryazov, P. O. Widmark, M. Cossi, B. Schimmelpfennig, P. Neogrady, and L. Seijo, *Comput. Mater. Sci.* **28**, 222 (2003).
- ⁹²H. Lischka, R. Shepard, F. B. Brown, and I. Shavitt, *Int. J. Quantum Chem.* **S15**, 91 (1981).
- ⁹³H. Lischka, R. Shepard, R. M. Pitzer, I. Shavitt, M. Dallos, T. Müller, P. G. Szalay, M. Seth, G. S. Kedziora, S. Yabushita, and Z. Y. Zhang, *Phys. Chem. Chem. Phys.* **3**, 664 (2001).
- ⁹⁴H. Lischka, R. Shepard, I. Shavitt, R. M. Pitzer, M. Dallos, T. Müller, P. G. Szalay, F. B. Brown, R. Ahlrichs, H. J. Boehm, A. Chang, D. C. Comeau, R. Gdanitz, H. Dachsel, C. Ehrhardt, M. Ernzerhof, P. Höchtel, S. Irlé, G. Kedziora, T. Kovar, V. Parasuk, M. J. M. Pepper, P. Scharf, H. Schiffer,

- M. Schindler, M. Schüler, M. Seth, E. A. Stahlberg, J.-G. Zhao, S. Yabushita, Z. Zhang, M. Barbatti, S. Matsika, M. Schuurmann, D. R. Yarkony, S. R. Brozell, E. V. Beck, J.-P. Blaudeau, M. Ruckebauer, B. Sellner, F. Plasser, and J. J. Szymczak, COLUMBUS, an *ab initio* electronic structure program, release 5.9.2, 2008, see www.univie.ac.at/columbus.
- ⁹⁵M. Barbatti, G. Granucci, M. Persico, M. Ruckebauer, M. Vazdar, M. Eckert-Maksić, and H. Lischka, *J. Photochem. Photobiol. A* **190**, 228 (2007).
- ⁹⁶M. Barbatti, G. Granucci, M. Ruckebauer, F. Plasser, J. Pittner, M. Persico, and H. Lischka, newton-x: a package for Newtonian dynamics close to the crossing seam, 2011, see www.newtonx.org.
- ⁹⁷D. Cremer and J. A. Pople, *J. Am. Chem. Soc.* **97**, 1354 (1975).
- ⁹⁸J. C. A. Boeyens, *J. Chem. Crystallogr.* **8**, 317 (1978).
- ⁹⁹M. Barbatti and S. Ullrich, *Phys. Chem. Chem. Phys.* **13**, 15492 (2011).
- ¹⁰⁰T. Fleig, S. Knecht, and C. Hättig, *J. Phys. Chem. A* **111**, 5482 (2007).
- ¹⁰¹M. R. Silva-Junior, M. Schreiber, S. P. A. Sauer, and W. Thiel, *J. Chem. Phys.* **133**, 174318 (2010).
- ¹⁰²G. Fogarasi, X. F. Zhou, P. W. Taylor, and P. Pulay, *J. Am. Chem. Soc.* **114**, 8191 (1992).
- ¹⁰³L. Serrano-Andrés and J. J. Serrano-Pérez, in *Handbook of Computational Chemistry*, edited by J. Leszczynski (Springer Verlag, New York, 2011), p. 485.
- ¹⁰⁴J. J. Szymczak, M. Barbatti, and H. Lischka, *Int. J. Quantum Chem.* **111**, 3307 (2011).
- ¹⁰⁵N. C. Handy and A. J. Cohen, *Mol. Phys.* **99**, 403 (2001).
- ¹⁰⁶J. F. Dobson, M. J. Bunker, and E. K. U. Gross, *Phys. Rev. Lett.* **79**, 1905 (1997).
- ¹⁰⁷A. Dreuw and M. Head-Gordon, *Chem. Rev.* **105**, 4009 (2005).
- ¹⁰⁸M. J. G. Peach, T. Helgaker, P. Salek, T. W. Keal, O. B. Lutnaes, D. J. Tozer, and N. C. Handy, *Phys. Chem. Chem. Phys.* **8**, 558 (2005).
- ¹⁰⁹R. Mitrić, U. Werner, and V. Bonačić-Koutecký, *J. Chem. Phys.* **129**, 164118 (2008).
- ¹¹⁰E. Tapavicza, A. M. Meyer, and F. Furche, *Phys. Chem. Chem. Phys.* **13**, 20986 (2011).
- ¹¹¹I. Tavernelli, E. Tapavicza, and U. Rothlisberger, *J. Mol. Struct.: THEOCHEM* **914**, 22 (2009).